THE JOURNAL OF BIOLOGICAL CHEMISTRY
Vol. 280, No. 4, Issue of January 28, pp. 2972–2980, 2005

Printed in U.S.A.

A Major Histocompatibility Complex·Peptide-restricted Antibody and T Cell Receptor Molecules Recognize Their Target by Distinct Binding Modes

CRYSTAL STRUCTURE OF HUMAN LEUKOCYTE ANTIGEN (HLA)-A1·MAGE-A1 IN COMPLEX WITH FAB-HYB3*

Received for publication, October 4, 2004, and in revised form, October 28, 2004
Published, JBC Papers in Press, November 10, 2004, DOI 10.1074/jbc.M411323200

Martin Hülsmeyer,[a,b] Patrick Chames,[b,c] Roman C. Hillig,[d,e] Robyn L. Stanfield,[f] Gerhard Held,[g] Pierre G. Coulie,[h] Claudia Alings,[a] Gabriele Wille,[d] Wolfram Saenger,[a] Barbara Uchanska-Ziegler,[d] Hennie R. Hoogenboom,[i] and Andreas Ziegler[d,j]

From the [a]Institut für Chemie/Kristallographie, Freie Universität Berlin, 14195 Berlin, Germany, [c]Cellectis, 93235 Romainville, France, the [d]Institut für Immungenetik, Charité-Universitätsmedizin Berlin, Campus Virchow-Klinikum, Humboldt-Universität zu Berlin, 14050 Berlin, Germany, the [f]Scripps Research Institute, Department of Molecular Biology, La Jolla, California 92037, [g]Medical Department I, Universität des Saarlandes, 66421 Homburg/Saar, Germany, the [h]Cellular Genetics Unit, Institute of Cellular Pathology, Université de Louvain, 1200 Brussels, Belgium, and [i]Merus BV, Utrecht, The Netherlands

Antibodies with T cell receptor-like specificity possess a considerable diagnostic and therapeutic potential, but the structural basis of the interaction between an antibody and an histocompatibility antigen has so far not been determined. We present here the crystal structure (at 2.15 Å resolution) of the recombinant, affinity-matured human antibody fragment Fab-Hyb3 bound to the tumor-associated human leukocyte antigen (HLA)/peptide complex HLA-A1·MAGE-A1. Fab-Hyb3 employs a diagonal docking mode resembling that of T cell receptors. However, other than these natural ligands, the antibody uses only four of its six complementarity-determining regions for direct interactions with the target. It recognizes the C-terminal half of the MAGE-A1 peptide, the HLA-A1 α1-helix, and N-terminal residues of the α2-helix, accompanied by a large tilting angle between the two types of molecules within the complex. Interestingly, only a single hydrogen bond between a peptide side chain and Fab-Hyb3 contributes to the interaction, but large buried surface areas with pronounced shape complementarity assure high affinity and specificity for MAGE-A1. The HLA-A1·MAGE-A1·antibody structure is discussed in comparison with those of natural ligands recognizing HLA·peptide complexes.

The adaptive immune system employs two principally different defense mechanisms in response to pathogens. Cell-mediated immune responses involve T cell receptors (TCRs)[1] that recognize proteolytic fragments processed from antigenic proteins in the context of class I or class II major histocompatibility (MHC) molecules (pMHC complexes) expressed on target cells. In contrast, humoral responses are characterized by the production of antibodies that react with individual, usually unprocessed foreign antigens, mostly glycoproteins and polysaccharides.

Soluble proteins endowed with a TCR-like specificity have a wide range of potentially useful applications, including direct visualization and quantification of pMHC complexes, and targeted delivery of toxins and drugs (1). Engineering of recombinant TCRs has not been very successful because of the low affinity (in the micromolar range) typically displayed by these molecules toward their targets, as well as a certain incompatibility with regard to manipulation of specificity and affinity (2, 3). Although antibodies are traditionally recognized as the tool of choice to achieve specific binding with high affinity (4), it has been exceptionally difficult to identify antibodies with "TCR-like" specificity following immunization procedures (5–13). However, *in vitro* selection of antibody fragments from large libraries displayed on the surface of filamentous phage has been shown to overcome the problems associated with the production of pMHC-restricted antibodies through immunization procedures (14–16).

We have previously been able to select a recombinant human Fab fragment (14) capable of binding specifically to a pMHC complex of considerable clinical interest, the tumor-associated HLA-A1·melanoma-associated antigen (MAGE)-A1 complex (17, 18). The initially isolated antibody, Fab-G8, displayed specificity for this pMHC but only moderate affinity. It was therefore subjected to phage display-based affinity maturation and screening to identify clones with a higher affinity and the same specificity (19). The best variant of Fab-G8, Fab-Hyb3 (or

* This work was supported in part by European Union Grant BMH4-CT98-3732; Deutsche Forschungsgemeinschaft Grant SFB449, projects B5 and B6, HE 3362/1-1; Berliner Krebsgesellschaft; Sonnenfeld-Stiftung Berlin; and Fonds der Chemischen Industrie. The costs of publication of this article were defrayed in part by the payment of page charges. This article must therefore be hereby marked "*advertisement*" in accordance with 18 U.S.C. Section 1734 solely to indicate this fact.

The atomic coordinates and structure factors (code 1W72) have been deposited in the Protein Data Bank, Research Collaboratory for Structural Bioinformatics, Rutgers University, New Brunswick, NJ (http://www.rcsb.org/).

[b] These authors contributed equally to this work.

[e] Present address: Schering AG, Research Laboratories, 10589 Berlin, Germany.

[j] To whom correspondence may be addressed: Institut für Immungenetik, Charité-Universitätsmedizin Berlin, Campus Virchow-Klinikum, Humboldt-Universität zu Berlin, Spandauer Damm 130,14050 Berlin, Germany. Tel.: 49-30-4505-53501; Fax: 49-30-4505-53953; E-mail: andreas.ziegler@charite.de.

[1] The abbreviations used are: TCR, T cell receptor; HLA, human leukocyte antigen; KIR, killer inhibitory immunoglobulin-like receptor; MHC, major histocompatibility complex; pMHC, major histocompatibility antigen complexed with a peptide; CDR, complementarity determining region; H, antibody heavy chain; L, antibody light chain; MAGE, melanoma-associated antigen; AMF complex, HLA-A1·MAGE-A1·Hyb3 complex; MES, 4-morpholineethanesulfonic acid.

short, Hyb3), exhibited a much higher affinity (K_d = 14 nM) as compared with G8 (K_d = 250 nM), yet maintained its peptide selectivity according to enzyme-linked immunosorbent assay tests and flow cytometry with phage-bound Fab and in T cell retargeting experiments (19, 20).

The structural basis of MHC-restricted peptide specificity has been well illustrated for TCRs (21), but thus far it remained unclear whether pMHC-specific antibodies would utilize a structurally similar or very different solution to achieve such specificity, in particular in light of their typically higher affinity for pMHC complexes as compared with TCRs. The plethora of different structural modalities described for antibody-antigen interactions (19, 22–24) does not permit a prediction to be made regarding the mode of interaction of HLA-A1·MAGE-A1 with Hyb3. Therefore, we decided to determine the structure of such a high affinity pMHC-restricted antibody in complex with its antigen. In this paper we describe the crystal structure of Hyb3 complexed with its target and discuss the similarities and differences in pMHC binding modes between this reagent and cellular ligands such as TCRs.

EXPERIMENTAL PROCEDURES

Protein Production—The MAGE-A1 peptide (EADPTGHSY) was solid phase synthesized and purified by high pressure liquid chromatography or purchased (Alta Bioscience, Birmingham, UK). HLA-A*010101·MAGE-A1 complexes were produced by refolding from *Escherichia coli* inclusion bodies (25) and purified by gel filtration using a Superdex 75HR column (Amersham Biosciences) as detailed previously (14). Fab-Hyb3 was expressed as described for Fab-G8 (14) and recovered from the *E. coli* cell pellet without the need for mechanical cell disruption by treatment with the mild protein extraction reagent B-PER (Pierce) and DNase I. It was then purified by affinity chromatography and gel filtration on Superdex 75 10/300 GL columns. Purified aliquots of HLA-A1·MAGE-A1 and Hyb3 were mixed at mass ratio 1:0.8, respectively, incubated at room temperature for 30 min, concentrated 4-fold using Millipore Ultrafree ultrafiltration units (Millipore, Schwalbach, Germany), and applied on a Superdex 75HR gel filtration column to remove excessive pMHC. The HLA-A1·MAGE-A1·Fab-Hyb3 (AMF) complex eluted as a symmetric peak with an apparent molecular mass of 94 kDa. SDS-PAGE confirmed the purity of the sample and the presence of all protein chains. The complex was concentrated to 15–20 mg/ml using a Millipore Ultrafree ultrafiltration device and employed for crystallization.

Crystallization and Data Collection—All of the crystallization experiments were performed by vapor diffusion using the hanging drop technique at 18 °C. Initially, needle clusters were obtained from a polyethylene glycol 4000-based screen (JBScreen3; Jena Biosciences, Jena, Germany). The crystals were very difficult to reproduce and responded strongly to small changes of the precipitant composition. After optimization, large rod-like clusters with individual rods up to 200 × 40 × 40 μm grew from drops of 0.7 μl of protein and 0.7 μl of precipitant (0.1 M MES, pH 6.5, 19% w/v polyethylene glycol 3350, 600 mM NaCl, 0.5% v/v dioxane). For data collection a suitable crystal was isolated from a cluster, soaked briefly in cryobuffer (precipitant solution plus 10% glycerol), and flash-cooled in liquid nitrogen. A native data set at 2.15 Å resolution was collected at beam line ID29 of the European Synchrotron Radiation Facility (Grenoble, France; λ = 0.9762 Å, MAR CCD detector). All of the measurements were performed at 100 K. The data were processed with the program DENZO and scaled with SCALEPACK (see Table I) (26).

Structure Determination—The structure of the AMF complex was determined by molecular replacement. As assessed from the Matthews coefficient, two complexes (I and II) were expected in the asymmetric unit (V_M = 2.1 Da/Å^3). HLA molecule (I) was unequivocally localized with a peptide-stripped HLA-A2 model (Protein Data Bank code 1duz) using Molrep from the CCP4 program suite (27). With molecule (I) fixed, HLA molecule (II) could be localized. After rigid body refinement (Refmac (27)), the R/R_{free} was 0.49/0.50. Hyb3 was located using a data base of 125 intact Fabs as search models. With AmoRe (27) Fab (I) was localized (with the two HLA molecules fixed) with Protein Data Bank code 7fab as search model. Because Fab (II) could not be unambiguously localized, the search was carried out with all Fab search models split into their variable and constant domains. Now the variable domain of Protein Data Bank code 2gfb was located, and subsequently a solution for the constant domain of Protein Data Bank code 2fb4 was found. This initial model was subjected to simulated annealing and energy minimization using CNS (28), automatic rebuilding using Arp/wArp (29), iterative cycles of manual rebuilding using O (30), and restrained maximum-likelihood refinement with Refmac. Noncrystallographic symmetry restraints were not applied at any time during refinement. Water molecules were included on the basis of peak heights (>2.5 σ in $F_o - F_c$ density maps) with ARP/wARP and manual fitting. After translation, libration, screw rotation refinement (31), the R value converged at 0.183 (R_{free} = 0.248) at 2.15 Å resolution. During structure determination, R_{free} served to control the process of convergence. The final model comprises 1632 protein and peptide residues, 653 water molecules, and 4 glycerol molecules. The stereochemistry of the refined structure was validated with Procheck (32) and Whatcheck (33). The figures were generated using Molscript (34) and raster3D (35) and other programs as indicated in the figure legends.

TABLE I
Data collection and refinement statistics

Data collection	
Space group	$P2_1$
Unit cell a (Å), b (Å), c (Å), and β (°)	125.4, 50.1, 136.7, 109.9
Resolution (Å)[a]	30.0–2.15 (2.23–2.15)
Unique reflections	78,453 (7786)
Redundancy	2.4 (2.2)
Completeness (%)[a]	90.0 (90.3)
I/σ[a]	15.1 (2.3)
R_{sym}[a,b]	0.055 (0.234)
Refinement	
Resolution (Å) [a]	30.0–2.15 (2.23–2.15)
Reflections (work set/test set)	74,477/3961
Nonhydrogen atoms/number of residues	13,455/1632
R_{cryst}[a,c]	0.183 (0.22)
R_{free}[a,d]	0.248 (0.27)
HLA-A1 heavy chain, no. of atoms/average B value (Å^2) (chain A/D)	2228/23.2/24.4
β_2-Microglobulin, no. of atoms/average B value (Å^2) (chain B/E)	837/24.9/26.4
MAGE-A1 peptide, no. of atoms/average B value (Å^2) (chain C/F)	69/21.6/23.8
Hyb3-H, no. of atoms/average B value (Å^2) (chain H/I)	1667/23.0/23.4
Hyb3-L, no. of atoms/average B value (Å^2) (chain L/M)	1586/23.1/22.9
Water, no. of molecules/average B value (Å^2)	653/37.5
Glycerol, no of atoms/average B value (Å^2)	24/51.9
Estimated overall coordinate error (Å)[e]	0.24
Root mean square deviation from ideal geometry	
Bond length (Å)	0.012
Bond angles (°)	1.6
Ramachandran plot	
Most favored regions (%)	90.3
Additionally allowed regions (%)	9.3
Disallowed regions (%)	0.4

[a] The values in parentheses refer to the highest resolution shell.
[b] $R_{sym} = \Sigma_{h\Sigma i} |I_{h,i} - \langle I_h \rangle| / \Sigma_{h\Sigma i} I_{h,i}$.
[c] $R_{cryst} = \Sigma_h |F_o - F_c| / \Sigma F_o$ (working set, no σ cut-off applied).
[d] R_{free} is the same as R_{cryst} but calculated on 5% of the data excluded from refinement.
[e] Estimated overall coordinate error based on R_{free} as calculated by Refmac 5.1.9999.

RESULTS

General Features of the HLA-A1·MAGE-A1·Hyb3 Complex—Crystals of the AMF complex diffracted synchrotron radiation to 2.15 Å resolution. The structure was determined by molecular replacement and refined to R/R_{free} values of 0.18/0.25 (Table I). There are two AMF complexes (I and II) per asym-

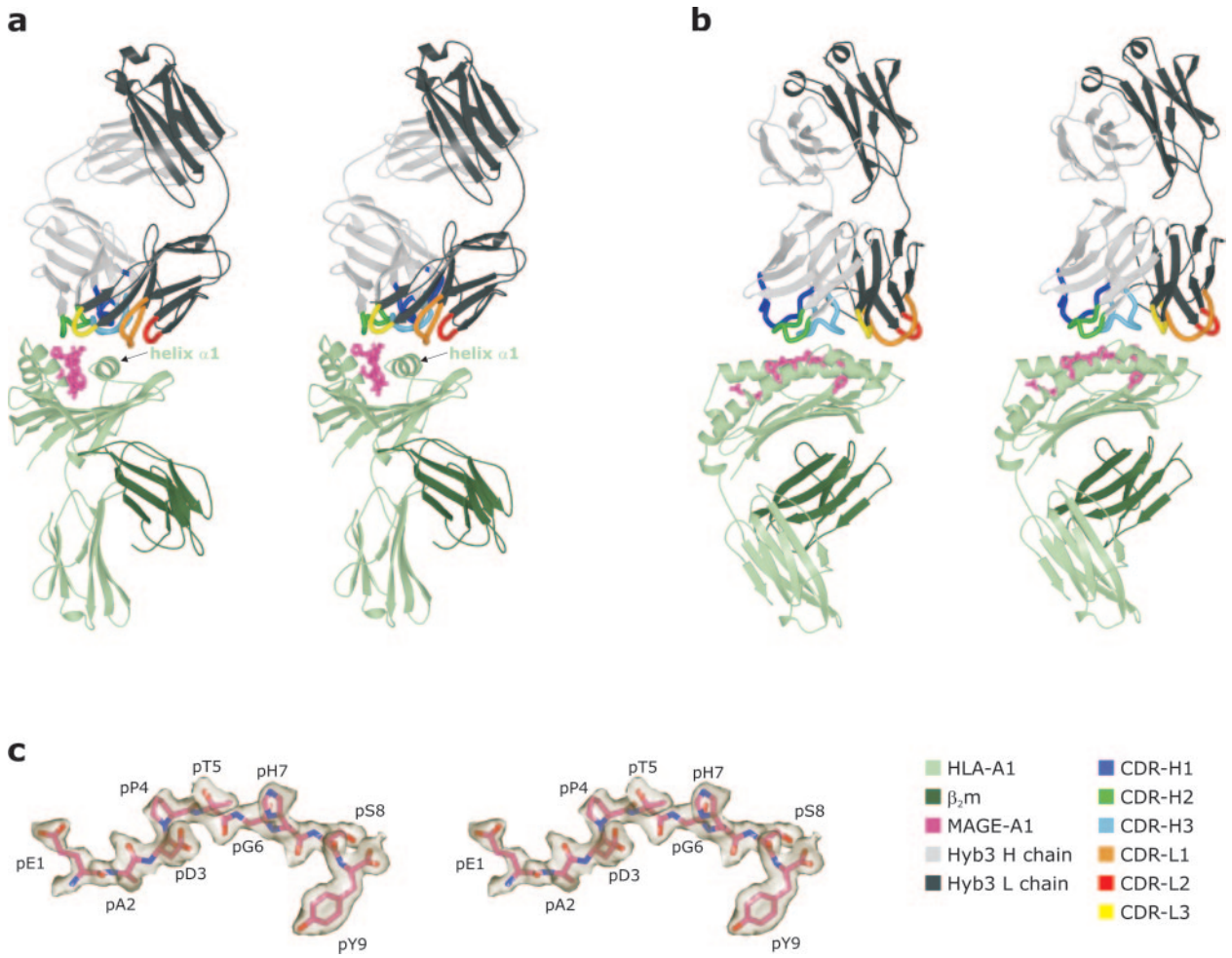

FIG. 1. **Overall topography of the AMF complex and conformation of the MAGE-A1 peptide.** Stereo views of the HLA-A1·MAGE-A1·Hyb3 complex viewed along the peptide axis, with the peptide C terminus in front (*a*) or rotated by 90° (*b*). The color code for CDR loops, pMHC and Fab is given in the legend. In *c* the final $2F_o - F_c$ electron density map of the MAGE-A1 peptide is shown at 1 σ contour level. The figure was generated using Povscript+ (www.stanford.edu/~fenn/povscript/).

metric unit, related by 2-fold noncrystallographic symmetry, and unless otherwise stated, the description and discussion will focus on complex I. The HLA-A*010101 (or short, HLA-A1) heavy chain, β_2-microglobulin, peptide, and Hyb3 heavy and light chains will be designated with chain identifiers A, B, P, H, L, respectively. Hyb3 H and L chains are numbered following the standard Kabat convention. Most parts of the structure are well ordered with only two HLA-A1 loops (Ala^{15}–Ala^{20} and Ala^{223}–Ala^{228}), the N-terminal Met of β_2-microglobulin, and Hyb3 residues His^{196}–His^{200} displaying substantial flexibility.

The overall topography of the HLA-A1·MAGE-A1 complex (Fig. 1, *a* and *b*) corresponds to previously determined pMHC structures (36). The MAGE-A1 peptide (EADPTGHSY, P1–P9) was modeled into the electron density without ambiguity (Fig. 1*c*). Its middle section (P4–P7) is only loosely bound to the peptide-binding groove of HLA-A1, a feature shared with most but not all pMHC class I complexes (36–39). A substantial amount of stabilization comes from water molecules in the proximity of the peptide that mediate additional contacts to the HLA-A1 heavy chain and the peptide. The HLA-A1·MAGE-A1 complex presents a relatively flat antigenic surface, because only one side chain (SerP8) points directly into the solvent (Fig. 1), whereas ProP4 and HisP7, although solvent-accessible, hardly protrude above the binding groove.

The Interface of HLA-A1·MAGE-A1 and Hyb3—The contribution to the binding interface is not distributed equally among the H and L chains of Hyb3 but in a 2-1 ratio. The complementarity determining region (CDR) loop CDR-H1 recognizes residues of the α1-helix and CDR-L3 interacts with both α-helices of HLA-A1·MAGE-A1, whereas CDR-H2 and CDR-H3 exhibit an intermediate position in that they contact both the peptide and the α1-helix. Marginal contributions come from CDR-L1 and CDR-L2 (in each case, distances >3.8 Å).

The most important interactions between Fab and pMHC are mediated by CDR-H3. This loop is rich in aromatic amino acids (^{98}FHYYYY^{100C}) (Fig. 2, *a* and *b*) and forms a clamp over the α1-helix with PheH98, TyrH100B, and TyrH100C on the external and HisH99 and TyrH100A on the internal side of the peptide binding groove (Fig. 2*b*). Solvent molecules are absent from this part of the interface, indicating strict shape complementarity. Residues with a buried surface area of >60 Å^2 are PheH98, HisH99, TyrH100A, TyrH100B, and TyrH100C from CDR-H3, as well as ArgA65 and GlnA72 from HLA-A1 (Fig. 2*a* and Tables II, III, and IV). In addition, HisH99 and TyrH100A are not only in contact with the α1-helix but are also hydrogen-bonded to the peptide, either directly or via buried water molecules (Fig. 2, *b* and *c*). The conformation of the CDR-H3 loop is further stabilized by an interaction between CDR-H1 and the HLA-A1 heavy chain, because AspH30 and AspH31 form hydrogen bonds with ArgA65 (Table II), thereby positioning it such that PheH98 of CDR-H3 can pack hydrophobically against the aliphatic section of the ArgA65 side chain. These interactions bury more than 100 Å^2 of ArgA65 surface area (Fig. 2*a*) and can be expected to provide a substantial contribution to the

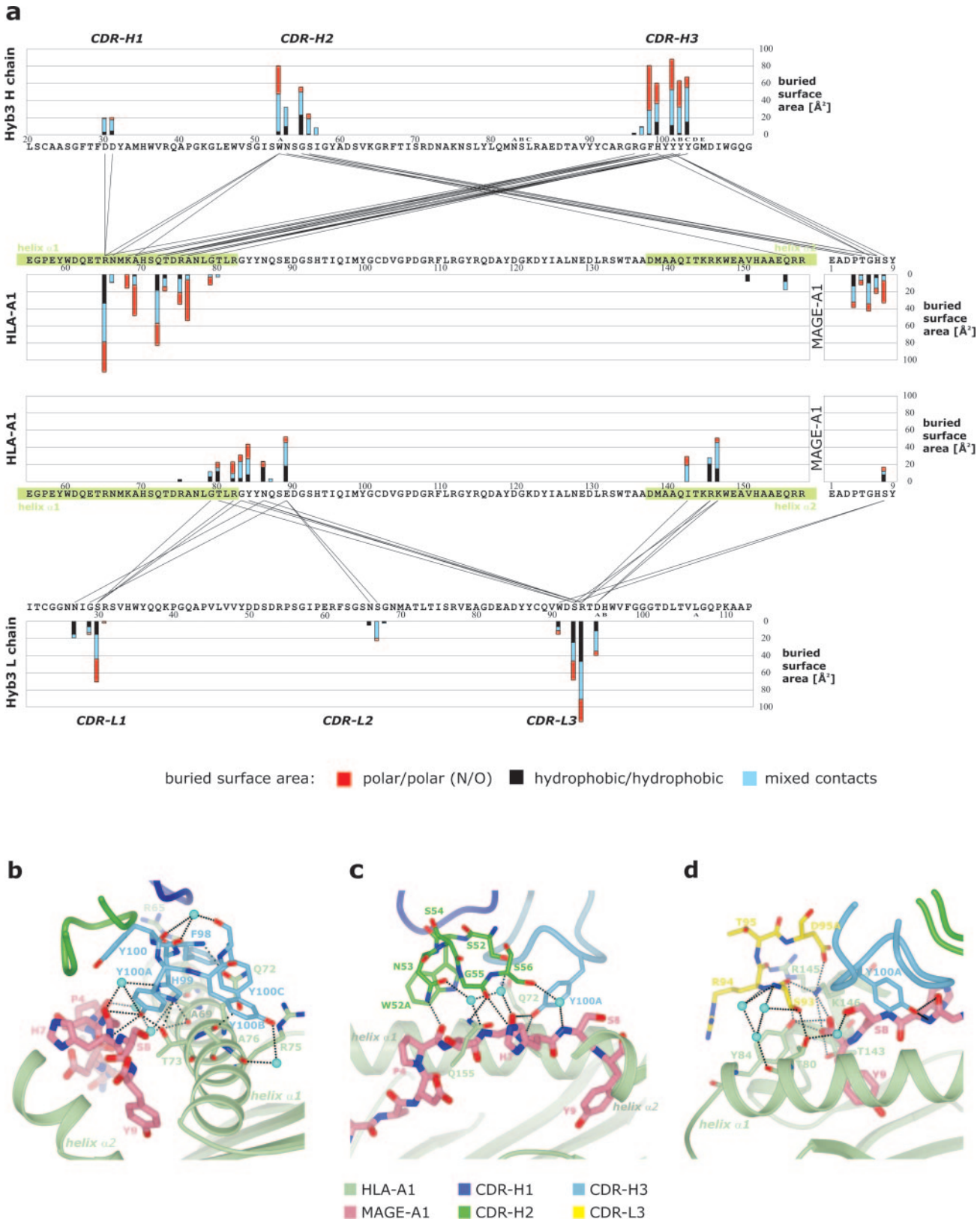

FIG. 2. **Interaction of the HLA-A1·MAGE-A1 complex with Hyb3.** *a*, linkage plot. The figure shows the amount of surface area (in Å²/residue; in case of Hyb3, numbering follows the Kabat data base) buried upon complex formation. Polar/polar contact areas (*N/O*) are shown as *red bars*, hydrophobic/hydrophobic contact areas (all other atoms) are shown as *black bars*, and mixed contact areas between polar atoms of one molecule and apolar atoms of the other are shown as *blue bars*. Residues which occlude each other are connected by *straight lines*. The locations of the CDR loops are indicated. α-Helices of the HLA-A1 molecule are colored *green*. *b–d*, examples for interactions. The color code for HLA-A1 heavy chain, peptide and CDR loops is given in the legend; water molecules are depicted as *blue spheres*, hydrogen bonds are depicted as *dotted lines*. The three panels depict the CDR-H3 clamp over the α1-helix (*b*), the CDR-H2 loop with the only direct interaction of Hyb3 with a peptide side chain (*c*), and the CDR-L3 loop interacting with residues in the vicinity of the C terminus of the peptide (*d*).

TABLE II
Direct contacts (≤3.5 Å) between Hyb3 and HLA-A1 heavy chain

Hyb3 element	Hyb3 contact atom	HLA-A1 contact atom	Distance
			Å
Hydrogen bonds			
CDR-H1	AspH30 O	ArgA65 NH1	2.9
	AspH30 OD1	ArgA65 NH1	3.4
	AspH31 OD1	ArgA65 NH1	3.0
CDR-H2	GlyH55 O	GlnA155 NE2	3.1
CDR-H3	PheH98 N	GlnA72 OE1	3.0
	HisH99 NE2	AlaA69 O	2.6
	HisH99 NE2	ThrA73 OG1	2.9
	TyrH100A OH	ThrA73 OG1	2.7
	TyrH100C OH	GlnA72 O	2.6
CDR-L3	SerL93 OG	ThrA80 OG1	2.5
	SerL93 O	LysA146 NZ	2.7
	ArgL94 O	ArgA145 NH2	3.2
	AspL95A OD1	LysA146 NZ	3.1
van der Waals' interactions			
CDR-H3	TyrH100B CG	AlaA76 CB	3.5
CDR-L3	SerL93 CB	Tyr80A CG2	3.5
	AspL95A CG	LysA146 CE	3.5

TABLE III
Hydrogen bonds (≤3.5 Å) between Hyb3 and MAGE-A1 peptide

Hyb3 element	Hyb3 contact atom	Peptide contact atom	Distance
			Å
CDR-H2	AsnH53 ND2	ProP4 O	2.8
	GlyH55 O	HisP7 NE2	3.3
CDR-H3	TyrH100A OH	GlyP6 O	3.1
	TyrH100A OH	HisP7 N	3.2

TABLE IV
Water-bridged contacts (≤3.5 Å) between Hyb3 and HLA-A1·MAGE-A1 complex

Hyb3 element	Hyb3 contact atom	Water molecule	pMHC contact atom	Distances
				Å
CDR-H2	TrpH52A NE1	Wat X4	ProP4 O	3.3/2.7
	AsnH53 OD1	Wat S37	GlyP6 N	2.8/2.9
	SerH56 OG	Wat S40	SerP8 N	2.8/3.0
CDR-H3	HisH99 ND2	Wat S36	GlyP6 O	2.8/2.8
	HisH99 NE2	Wat Z43	Ala69 O	3.4/3.2
CDR-L2	GlyL68 N	Wat Z55	GluA89 OD1	3.0/2.6

affinity of Hyb3 toward the HLA-A1·MAGE-A1 complex. A number of hydrogen bonds to the MAGE-A1 peptide are formed by the CDR-H2 loop (Fig. 2, *a* and *c*, and Table III), mostly to the peptide backbone, either directly or mediated by interconnecting water molecules. Furthermore, this loop provides the sole contact to the central region of the α2-helix (Fig. 2*c* and Table II). Another important component contributing to the interaction of HLA-A1·MAGE-A1 and Hyb3 is CDR-L3, which spans across the end of the binding groove where the peptide C terminus is located (Fig. 2, *a* and *d*, and Table II). It includes a salt bridge from AspL95A to LysA146.

The resolution of the AMF data set was sufficient to permit the identification of 653 water molecules, of which six are completely buried in the AMF interface (Table IV) and contribute substantially to the high shape complementarity. The median value of the shape complementarity statistic (*Sc*) is a measure of the geometric match at protein-protein interfaces (40). For the AMF complex, *Sc* is 0.69 excluding and 0.72 including water molecules in the interface. These values are very close to those from the two structures of killer inhibitory immunoglobulin-like receptors (KIR) complexed with HLA-C (0.69 and 0.71, respectively) (41, 42), in contrast to pMHC·TCR interactions that reveal widely varying *Sc* values (0.43–0.70) (43–47). Additional water molecules in clefts and crevices near the interacting surfaces mediate further hydrogen bonds and extend the protein·protein interface (Fig. 3*a*). The importance of the bound water molecules is also evident from a two-dimensional projection of the atom-to-atom distance (Fig. 3*b*) and the polarity (Fig. 3*c*) of the interface.

Hyb3 is the outcome of a complex *in vitro* affinity maturation process (19), starting from the lower affinity Fab-G8 (14). In the absence of a structure for Fab-G8, it is difficult to assess which individual mutations contribute most to the affinity increase of Hyb3. There are only two amino acid substitutions between the H chains of G8 and Hyb3 (both in the CDR-H3 region; Fig. 4*a*), but neither of them is directly involved in contacting the HLA-A1·MAGE-A1 complex (Fig. 2*a* and Tables II, III, and IV). A completely different situation is found regarding the L chains of G8 and Hyb3. By L chain shuffling, 22 residues (*i.e.* about 20% of the V region residues) were exchanged, more than half of them outside of CDR loops (Fig. 4*a*). ArgL94 is the only Hyb3 residue with a buried surface larger than 100 $Å^2$ (Fig. 2*a*), thus representing one of the crucial contact residues. In G8, this residue is a Thr (Fig. 4). The mutation seems to have optimized hydrophilic as well as hydrophobic contacts to the pMHC α-helices, leading to an increased amount of buried surface and improved complementarity (Figs. 3*a* and 4*b*).

Comparison of the AMF with Other pMHC·Ligand Complexes—Although TCRs seem to be restricted to one common pMHC binding mode (21, 48), in principle one could imagine numerous modes by which an antibody could bind to a pMHC

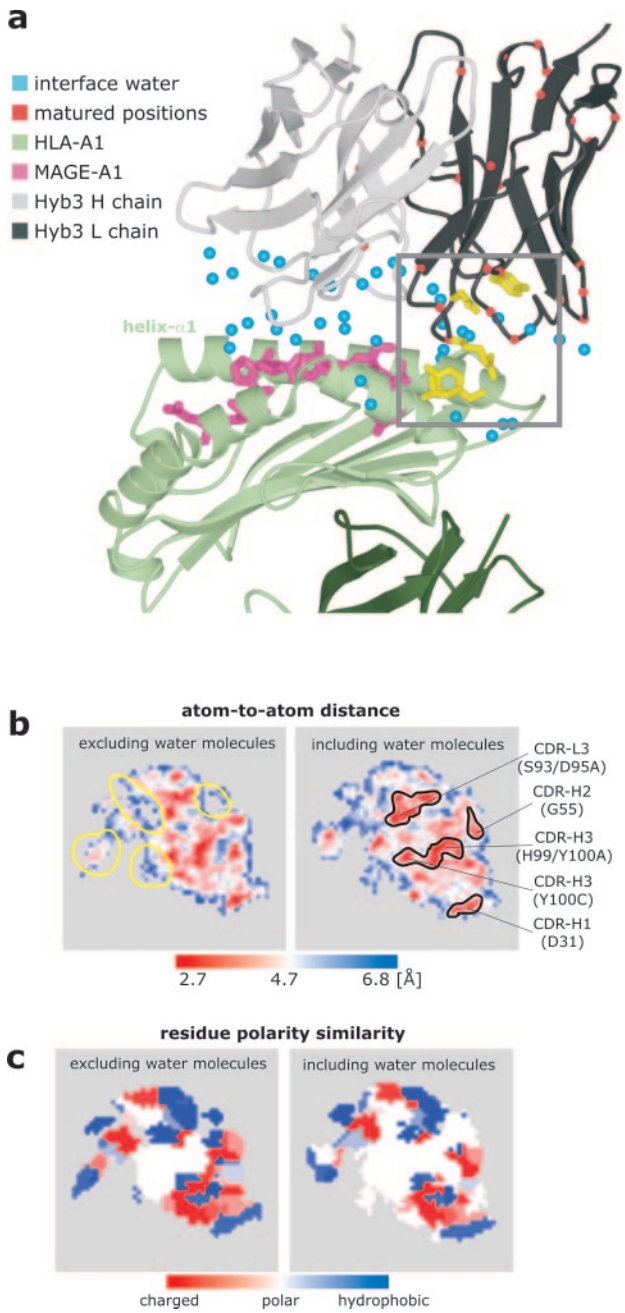

FIG. 3. **Water molecules at the HLA-Fab interface.** *a* shows an enlarged view of the interface region of HLA-A1·MAGE-A1 (binding groove area with the peptide in place) and Hyb3 (variable domains) together with interfacial waters depicted as blue spheres. The color code of the protein complex is given in the legend. All of the residues that changed during the maturation process from G8 to Hyb3 are highlighted with *red dots*. The *box* marks the region that is depicted in close-up view in Fig. 4*b*. *b*, two-dimensional projection of interface properties of the HLA-A1·MAGE-A1·Hyb3 complex illustrating the atom-to-atom distance between HLA and Fab as small (*red*) and large (blue) (see legend). Binding hot spots are *circled* in *black*. Regions that change substantially after inclusion of water molecules are *circled* in *yellow*. In *c* the residue polarity similarity is mapped on the two-dimensional surface projection. The interface is characterized mainly by polar interactions. Water molecules contribute markedly to the overall characteristic of the interaction. The figure was generated using *Molsurfer* (projects.villa-bosch.de/dbase/molsurfer/).

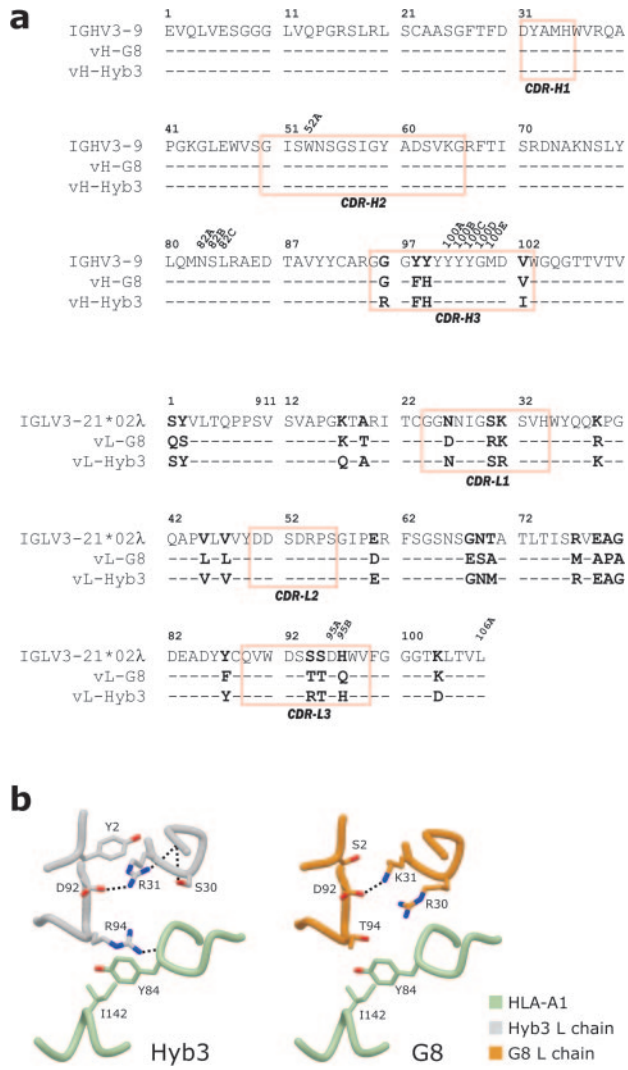

FIG. 4. **Comparison of G8 with Hyb3.** *a*, sequence alignment of the V_H and V_L domains of the G8 and Hyb3 molecules with their most closely related V regions, respectively, from the Kabat data base. Residue exchanges associated with maturation are highlighted with *bold letters*, and the locations of the CDR regions are indicated by *red boxes*. *b*, close-up views of an interesting matured region of the Hyb3 and G8 L chain outlined by the *gray box* in Fig. 3*a*. In this area several residues are exchanged, giving rise to enhanced affinity. Backbone segments are depicted as *thick coils* with selected side chains in stick presentation. Hydrogen bonds are depicted as *dotted lines*. The figure showing the G8 section was generated by manually modeling mutated residues.

in a peptide-specific manner. However, the interactions of Hyb3 with HLA-A1·MAGE-A1 resemble those of TCRs with pMHCs in several respects (Fig. 1, *a* and *b*). In particular, Hyb3 docks from the "top" to an epitope encompassing the flat surface composed of the helices and the antigenic peptide. Also, the diagonal binding mode between the two partners within the AMF complex resembles that observed in the pMHC·TCR complexes determined so far.

However, the overall architecture of the AMF complex is different as the tilting angle τ (see definition in legend of Fig. 5) between HLA-A1 and Hyb3 is 45° but is found much smaller, in the range of 7–14°, for pMHC·TCR complexes (43–46). In addition, the orientation of Hyb3 with respect to the pMHC differs from those found for pMHC·TCR complexes as revealed by the footprints in Fig. 5 (*b–f*). Although TCRs usually bind to the center of the pMHC peptide binding groove and to adjacent parts of the α1- and α2-helices, the position of Hyb3 and associated binding interactions are shifted toward the α1-helix and toward the peptide C terminus (Fig. 5, *b* and *c*). The two types of epitopes overlap, however, and this is found also when the Hyb3 footprint on HLA-A1·MAGE-A1 is compared with those of two KIRs on HLA-C molecules (Fig. 5, *c* and *g*) (41, 42).

Hyb3 recognizes the MAGE-A1 peptide via the CDR-H2 and

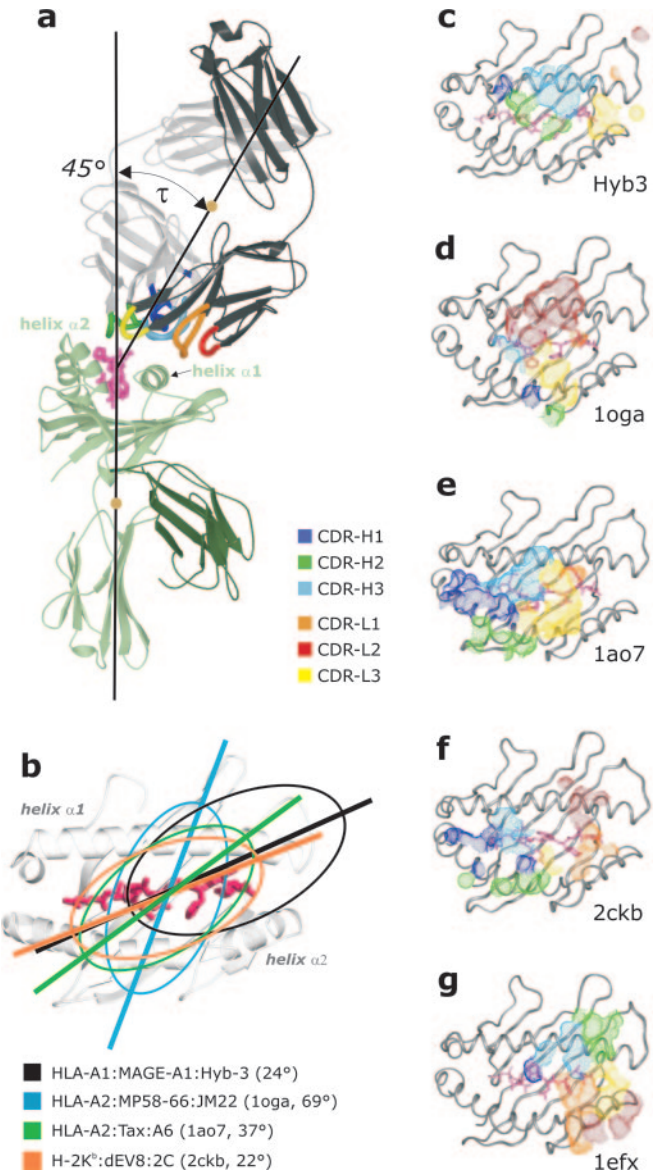

FIG. 5. **Comparison of Hyb3, TCR, and KIR binding modes with pMHCs.** *a* illustrates the definition of the tilting angle τ of the Fab on top of the HLA molecule. The *lines* passing through the centers-of-mass (*orange circles*) of the two interaction partners and the center of the peptide (C_α at P5) are used to calculate the angle τ between these two lines. Typically, small τ angles (7–14°) are found in pMHC·TCR complexes (see text). *b*, comparison of the binding orientation of Hyb3 in the AMF complex with that of pMHC·TCR complexes. The angles are calculated from an axis between the disulfide bridges of the V_L and V_H domains of Hyb3 (or Vα and Vβ of a TCR) and the axis spanning the N and C termini of the cognate peptide. The ellipses refer to the bodies of the Hyb3 or TCR molecule, respectively, schematically projected on the binding groove. TCR binding interactions are focused on the center of the peptide and the binding groove, whereas they are shifted toward the α1-helix with Hyb3. *c–g*, footprints of the CDR loops of Hyb3, the Vα and Vβ chains of three TCRs, and interacting loops of a KIR on pMHCs. Surfaces of atoms within 4 Å distance to the pMHC are shown in colors corresponding to the respective CDR loops (see legend). The view is from the Fab, TCR, or KIR onto the peptide-binding site of the pMHC. The MHC binding groove is shown as C_α ribbon (*gray*); the peptide is in stick representation (*red*). *c*, Hyb3 footprint, color-coded according to the respective CDR loops and following Fig. 1. *d–f*, TCR footprints shown for comparison: Protein Data Bank codes 1oga (*d*), 1ao7 (*e*), and 2ckb (*f*). Color coding according to the respective CDR loops of the TCR Vα- and Vβ-chains as for the Hyb3 CDR-H and CDR-L loops. *g*, footprint of KIR2DL2 on HLA-Cw3 (Protein Data Bank code 1efx) with coloring in analogy to Hyb3 CDR loops: *dark blue* for residues 20–23, *green* for residues 43–46, *light blue* for residues 67–74, *orange* for residues 103–108, *red* for residues 130–135, and *yellow* for residues 182–184. Every type of ligand has found its individual solution for pMHC recognition.

CDR-H3 loops (Fig. 2, *b* and *c*) and contacts the pMHC via all H chain CDRs as well as via CDR-L3 (Fig. 5*c* and Tables II, III, and IV). By contrast, TCRs commonly use the CDR3 loops of their α- and β-chains for contacting the peptide, whereas the remaining CDRs bind to the α1- and α2-helices of a pMHC (see Fig. 5 (*d–f*) for selected examples). KIRs are comparable with TCRs with regard to the number of loops used for contacting a pMHC (Fig. 5*g*), although the location of these loops within the two Ig domains is completely different (41, 42). For the AMF complex, the buried molecular surface is 1930 Å^2, a value that lies within the typical range for pMHC·TCR complexes (HLA-A2·MP·JM22, Protein Data Bank code 1oga (46), 1550 Å^2; HLA-A2·Tax·A6, Protein Data Bank code 1ao7 (43), 2020 Å^2; H-2K^b·dEV8·2C, Protein Data Bank code 2ckb (44), 2080 Å^2) (Fig. 5, *d–f*) but is significantly larger than that for a typical protein·antibody interaction, which is about 1500 Å^2 (49). On the other hand, the HLA-C·KIR2DL2 interaction (Protein Data Bank code 1efx) buries only 1560 Å^2 of surface area (Fig. 5*g*) (41).

DISCUSSION

There are two central questions that our study addresses: (i) how are high affinity and specificity of the interaction between a pMHC-restricted antibody and its target achieved, and (ii) do pMHC-restricted antibodies share structural features with natural ligands in their binding mode to pMHC complexes? Despite the lack of specific docking points on the relatively featureless HLA-A1·MAGE-A1 surface (Figs. 1 and 2), the antibody Hyb3 recognizes the pMHC complex in a way that resembles those of TCRs with pMHCs in a number of respects. Three residues in the MAGE-A1 peptide have side chains that could act as hydrogen bonding partners for Hyb3 (TyrP5, HisP7, and SerP8). However, all direct contacts to the peptide are formed between side chains of the CDR loops of the antibody and peptide backbone atoms, except for HisP7^{NE2}, which hydrogen bonds to GlyH55^O (Fig. 2 and Tables II, III, and IV). The side chains of the other residues of the peptide are apolar and small (AlaP2, ProP4, and GlyP6) or are part of buried anchor positions (GluP1 and TyrP9).

Under these conditions, peptide specificity appears to be achieved by many close interactions to the peptide backbone that would be broken if another peptide such as MAGE-A3 (EVDPIGHLY, differing from MAGE-A1 at positions P2, P5, and P8) (14) were presented. Indeed, Hyb3 does not bind to HLA-A1 complexed to the MAGE-A3 peptide. It binds only weakly when this peptide carries Ser at position P8 and strongly when it carries Thr at position P5 (19). Further evidence supporting the importance of residues ThrP5 and HisP7 in the interaction comes from recent T cell retargeting experiments (20) with Hyb3, using alanine mutants of the MAGE-A1 peptide. It was found that alanine replacements at positions P5 and P7 abolish Hyb3-mediated cell killing, whereas its introduction at positions P1, P4, and P8 had no effect.[2]

In most of the pMHC-TCR structures reported, one or two residues protrude form the central peptide bulge and are contacted by the TCR, thus making an important contribution to specificity. This is somewhat different in the complex of HLA-A2·MP·JM22 (Protein Data Bank code 1oga) (46), in which the displayed peptide has no protruding side chains. The JM22 TCR overcomes this difficulty by delivering a "protrusion" by itself. The normal binding situation (protrusion from the peptide, notch/pit from the TCR) is inverted because of paucity of peptide side chains. In the case of Hyb3, we find a similar situation; protruding peptide side chains are missing here as well, and the antibody, by using the same strategy as JM22,

[2] R. Willemsen, personal communication.

also binds to a notch between the α1-helix and the peptide via its CDR-H3 region. Further peptide selectivity of Hyb3 is based on the direct contact of GlyH55 with GlnA155 and relies also on water molecules that act as small "adapters" to provide additional contacts between peptide and Hyb3 (Tables II and IV). Specificity for the HLA-A1 allele may be achieved by comparable interactions. The degree of allele specificity exhibited by Hyb3 has not been determined in detail (14), but HLA-A1 is distinguished by the presence of AlaA76 from nearly all other HLA class I heavy chains (www.ebi.ac.uk/imgt/hla/).

Previous structural studies of affinity-matured antibodies (50–52) have indicated that burial of increasing amounts of apolar surface, in particular at the interface periphery, and improved shape complementarity are the key structural elements that contribute to high affinity and specificity. In the absence of the pMHC·G8 structure, we cannot verify whether the maturation process in fact results in an increase of buried nonpolar surface, although the mutations that distinguish the H chain of G8 from that of Hyb3 (Arg^{96} and Ile^{102}) do occur in the periphery of the interface. The affinity increase caused by L chain mutations appears to arise mainly from indirect effects that stabilize the conformation of the CDR loops (Fig. 4).

Although still poorly understood, the characteristic diagonal docking mode for most pMHC·TCR interactions is thought to be due either to evolutionary pressure that shapes TCR V-gene repertoires or positive and negative T cell selection processes within the thymus, in which accessory proteins on the T cell surface might only be able to participate when the pMHC·TCR binding mode is appropriate (53, 54). Furthermore, TCRs with high affinity for foreign pMHC are negatively selected, thereby biasing T cell responses to interactions involving low affinity TCRs (55). These biological restraints, however, do not play a role for the selection of phage display-derived antibodies such as Hyb3 that are generated entirely *in vitro*. Nevertheless, a diagonal docking interaction characterizes also the AMF complex (Fig. 5). This cannot be regarded as surprising because, of the many ways in which a pMHC-specific antibody might be able to recognize its target, a diagonal binding mode is much more probable than an orientation of the Fab precisely in line with or perpendicular to the peptide. On the other hand, the *in vitro* selection process will enrich antibodies that have already established optimal contacts with the heavy chain and the peptide, without restricting the contribution of individual CDR loops to particular regions on the surface of a given pMHC, as in the case of TCRs (43–46). Therefore, the large tilting angle τ between Hyb3 and the HLA-A1·MAGE-A1 complex (Figs. 1 and 5) is probably a consequence of more interactions of Hyb3 with the α1- than the α2-helix of this pMHC.

The issue of pMHC recognition by TCRs and antibodies has also been addressed by Stryhn *et al.* (56) and by Messaoudi and co-workers (57) and more recently by Biddison *et al.* (24), who systematically compared the binding of several phage display-derived antibody fragments and TCRs recognizing the Tax or M1 peptides in the context of HLA-A2 and various heavy chain mutants. These studies reveal that both antibody fragments and TCRs were negatively affected by exchanges of residues in the vicinity of the N-terminal half of the peptide. In particular, mutations of HLA-A2 heavy chain Arg^{65} and Lys^{66} (Tax peptide) or Lys^{66} and Gln^{155} (M1 peptide) reduced or even abrogated TCR and Fab reactivity, implying an overlap of Fab footprints with those of TCR α-chains (24). ArgA65 and GlnA155 play a role in the AMF interaction as well, suggesting that the epitopes of the HLA-A2-specific Fabs might partially overlap with that of Hyb3 (Fig. 2). Conversely, results from two monoclonal antibodies and H-$2K^b$ molecules presenting an ovalbumin-derived peptide indicated that the antibody and the α-chain of the single TCR analyzed (57) shared parts of their footprints that are similar to KIR footprints on HLA-C·peptide complexes (Fig. 2) (41, 42). A detailed comparison is currently precluded because the structures of only a limited number of pMHC·ligand complexes are known.

In conclusion, our study provides a rationale for achieving a high affinity interaction, accompanied by a pronounced degree of specificity, between an antibody and a particular pMHC complex, even with a peptide that contributes only modestly to the epitope. The solution chosen by Hyb3 is to generate an extended paratope displaying a high surface complementarity with its epitope, through the formation of a binding hot spot on one α-helix and some key interactions on accessible parts of the peptide to ensure peptide selectivity. Structural studies of additional complexes of pMHC and antibodies will reveal to what extent the findings reported here can be generalized.

REFERENCES

1. Engberg, J., Krogsgaard, M., and Fugger, L. (1999) *Immunotechnology* **4,** 273–278
2. Wülfing, C., and Plückthun, A. (1994) *J. Mol. Biol.* **242,** 655–669
3. Holler, P. D., Holman, P. O., Shusta, E. V., O'Herrin, S., Wittrup, K. D., and Kranz, D. M. (2000) *Proc. Natl. Acad. Sci. U. S. A.* **97,** 5387–5392
4. Winter, G., and Milstein, C. (1991) *Nature* **349,** 293–299
5. van Leeuwen, A., Goulmy, E., and van Rood, J. J. (1979) *J. Exp. Med.* **150,** 1075–1083
6. Abastado, J. P., Darche, S., Jouin, H., Delarbre, C., Gachelin, G., and Kourilsky, P. (1989) *Res. Immunol.* **140,** 581–594
7. Aharoni, R., Teitelbaum, D., Arnon, R., and Puri, J. (1991) *Nature* **351,** 147–150
8. Murphy, D. B., Rath, S., Pizzo, E., Rudensky, A. Y., George, A., Larson, J. K., and Janeway, C. A., Jr (1992) *J. Immunol.* **148,** 3483–3491
9. Uchanska-Ziegler, B., Nössner, E., Schenk, A., Ziegler, A., and Schendel, D. J. (1993) *Eur. J. Immunol.* **23,** 734–738
10. Eastman, S., Deftos, M., DeRoos, P. C., Hsu, D. H., Teyton, L., Braunstein, N. S., Hackett, C. J., and Rudensky, A. (1996) *Eur. J. Immunol.* **26,** 385–393
11. Andersen, P. S., Stryhn, A., Hansen, B. E., Fugger, L., Engberg, J., and Buus, S. (1996) *Proc. Natl. Acad. Sci. U. S. A.* **93,** 1820–1824
12. Porgador, A., Yewdell, J. W., Deng, Y., Bennink, J. R., and Germain, R. N. (1997) *Immunity* **6,** 715–726
13. Dadaglio, G., Nelson, C. A., Deck, M. B., Petzold, S. J., and Unanue, E. R. (1997) *Immunity* **6,** 727–738
14. Chames, P., Hufton, S. E., Coulie, P. G., Uchanska-Ziegler, B., and Hoogenboom, H. R. (2000) *Proc. Natl. Acad. Sci. U. S. A.* **97,** 7969–7974
15. Lev, A., Denkberg, G., Cohen, C. J., Tzukerman, M., Skorecki, K. L., Chames, P., Hoogenboom, H. R., and Reiter, Y. (2002) *Cancer Res.* **62,** 3184–3194
16. Denkberg, G., Cohen, C. J., Lev, A., Chames, P., Hoogenboom, H. R., and Reiter, Y. (2002) *Proc. Natl. Acad. Sci. U. S. A.* **99,** 9421–9426
17. van der Bruggen, P., Traversari, C., Chomez, P., Lurquin, C., De Plaen, E., van den Eynde, B., Knuth, A., and Boon, T. (1991) *Science* **254,** 1643–1647
18. Maeurer, M. J., Storkus, W. J., Kirkwood, J. M., and Lotze, M. T. (1996) *Melanoma Res.* **6,** 11–24
19. Chames, P., Willemsen, R. A., Rojas, G., Dieckmann, D., Rem, L., Schuler, G., Bolhuis, R. L., and Hoogenboom, H. R. (2002) *J. Immunol.* **169,** 1110–1118
20. Willemsen, R. A., Debets, R., Hart, E., Hoogenboom, H. R., Bolhuis, R. L., and Chames, P. (2001) *Gene Ther.* **8,** 1601–1608
21. Rudolph, M. G., and Wilson, I. A. (2002) *Curr. Opin. Immunol.* **14,** 52–65
22. Wilson, I. A., and Stanfield, R. L. (1994) *Curr. Opin. Struct. Biol.* **4,** 857–867
23. Cohen, C. J., Denkberg, G., Lev, A., and Reiter, Y. (2003) *J. Mol. Recogn.* **16,** 324–332
24. Biddison, W. E., Turner, R. V., Gagnon, S. J., Lev, A., Cohen, C. J., and Reiter, Y. (2003) *J. Immunol.* **171,** 3064–3074
25. Garboczi, D. N., Hung, D. T., and Wiley, D. C. (1992) *Proc. Natl. Acad. Sci. U. S. A.* **89,** 3429–3433
26. Otwinowski, Z., and Minor, W. (1997) *Methods Enzymol.* **276,** 307–326
27. Collaborative Computational Project Number 4 (1994) *Acta Crystallogr. Sect. D Biol. Crystallogr.* **50,** 760–763
28. Brünger, A. T., Adams, P. D., Clore, G. M., DeLano, W. L., Gros, P., Grosse-Kunstleve, R. W., Jiang, J. S., Kuszewski, J., Nilges, M., Pannu, N. S., Read, R. J., Rice, L. M., Simonson, T., and Warren, G. L. (1998) *Acta Crystallogr. Sect. D Biol. Crystallogr.* **54,** 905–921
29. Perrakis, A., Morris, R., and Lamzin, V. S. (1999) *Nat. Struct. Biol.* **6,** 458–463
30. Jones, T. A., and Kjeldgaard, M. (1997) *Methods Enzymol.* **277,** 173–208
31. Winn, M. D., Isupov, M. N., and Murshudov, G. N. (2001) *Acta Crystallogr. Sect. D Biol. Crystallogr.* **57,** 122–133
32. Laskowski, R. A., MacArthur, M. W., Moss, D. S., and Thornton, J. M. (1995) *J. Appl. Crystallogr.* **26,** 283–291
33. Hooft, R. W., Vriend, G., Sander, C., and Abola, E. E. (1996) *Nature* **381,** 272
34. Kraulis, P. J. (1991) *J. Appl. Crystallogr.* **24,** 946–950
35. Merritt, E. A., and Bacon, D. J. (1997) *Methods Enzymol.* **277,** 505–524
36. Madden, D. R. (1995) *Annu. Rev. Immunol.* **13,** 587–622
37. Menssen, R., Orth, P., Ziegler, A., and Saenger, W. (1999) *J. Mol. Biol.* **285,** 645–653
38. Apostolopoulos, V., Yu, M., Corper, A. M., Li, W., McKenzie, I. F., Teyton, L., and Wilson, I. A. (2002) *J. Mol. Biol.* **318,** 1307–1316
39. Hülsmeyer, M., Fiorillo, M. T., Bettosini, F., Sorrentino, R., Saenger, W., Ziegler, A., and Uchanska-Ziegler, B. (2004) *J. Exp. Med.* **199,** 271–281

40. Lawrence, M. C., Coleman, P. M. (1993) *J. Mol. Biol.* **234,** 946–950
41. Boyington, J. C., Motyka, S. A., Schuck, P., Brooks, A. G., and Sun, P. D. (2000) *Nature* **405,** 537–543
42. Fan, Q. R., Long, E. O., and Wiley, D. C. (2001) *Nat. Immunol.* **2,** 452–460
43. Ding, Y. H., Smith, K. J., Garboczi, D. N., Utz, U., Biddison, W. E., and Wiley, D. C. (1998) *Immunity* **8,** 403–411
44. Garcia, K. C., Degano, M., Pease, L. R., Huang, M., Peterson, P. A., Teyton, L., and Wilson, I. A. (1998) *Science* **279,** 1166–1172
45. Ding, Y. H., Baker, B. M., Garboczi, D. N., Biddison, W. E., and Wiley, D. C. (1999) *Immunity* **11,** 45–56
46. Stewart-Jones, G. B., McMichael, A. J., Bell, J. I., Stuart, D. I., and Jones, E. Y. (2003) *Nat. Immunol.* **4,** 657–663
47. Ysern, X., and Mariuzza, R. A. (1998) *Nat. Struct. Biol.* **5,** 412–414
48. Housset, D., and Malissen, B. (2003) *Trends Immunol.* **24,** 429–437
49. Jones, S., and Thornton, J. M. (1996) *Proc. Natl. Acad. Sci. U. S. A.* **93,** 13–20
50. Li, Y., Li, H., Yang, F., Smith-Gill, S. J., Mariuzza, R. A. (2003) *Nat. Struct. Biol.* **10,** 482–488
51. Sundberg, E. J., Andersen, P. S., Schlievert, P. M., Karjalainen, K., and Mariuzza, R. A. (2003) *Structure* **11,** 1151–1161
52. Zahnd, C., Spinelli, S., Luginbühl, B., Amstutz, P., Cambillau, C., and Plückthun, A. (2004) *J. Biol. Chem.* **279,** 18870–18877
53. Buslepp, J., Wang, H., Biddison, W. E., Appella, E., and Collins, E. J. (2003) *Immunity* **19,** 595–606
54. Malissen, B. (2003) *Immunity* **19,** 463–464
55. Holler, P. D., Chlewicki, L. K., and Kranz, D. M. (2003) *Nat. Immunol.* **4,** 55–62
56. Stryhn, A., Andersen, P. S., Pedersen, L. O., Svejgaard, A., Holm, A., Thorpe, C. J., Fugger, L., Buus, S., and Engberg, J. (1996) *Proc. Natl. Acad. Sci. U. S. A.* **93,** 10338–10342
57. Messaoudi, I., LeMaoult, J., and Nikolić-Žugić, J. (1999) *J. Immunol.* **163,** 3286–3294